

Supplementary Information for

Long-Range Conductivity in Proteins Mediated by Aromatic ResiduesSiddharth Krishnan¹, Aleksei Aksimentiev^{1†}, Stuart Lindsay^{2,3,4*} and Dmitry Matyushov^{2,3†}

¹Department of Physics, and Beckman Institute for Advanced Science and Technology, University of Illinois at Urbana Champaign, Urbana, IL 61801, USA. ²Department of Physics, ³School of Molecular Sciences and ⁴Biodesign Institute, Arizona State University, Tempe, AZ 85281, USA

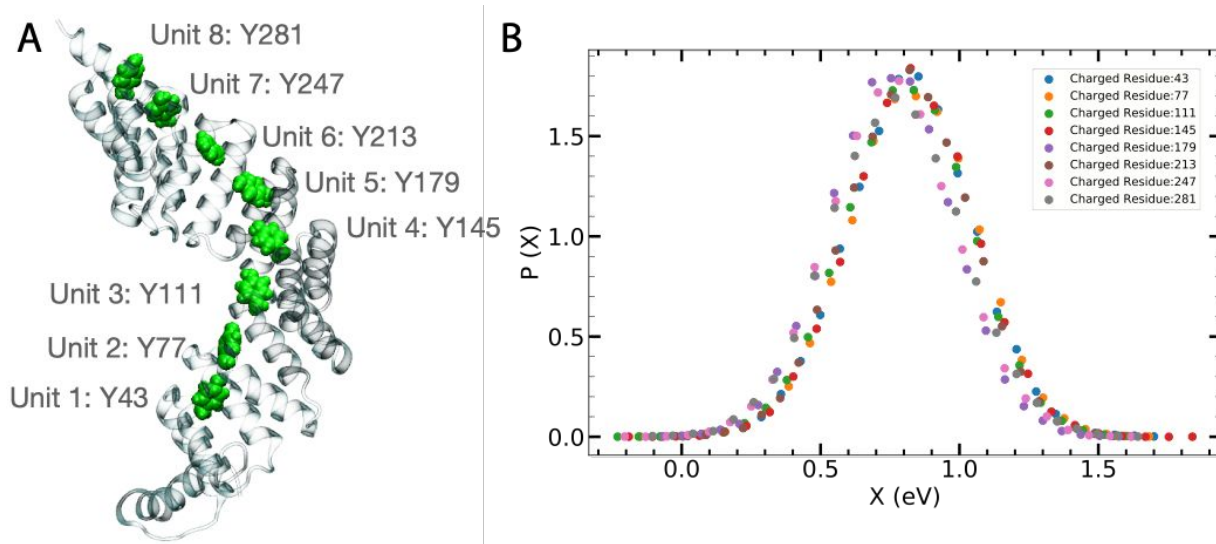


Figure S1. Energy gap fluctuations of equivalent residues in CTPR. A) Y43 and its equivalent residues in the eight repeat units of CTPR8. The sidechain of the equivalent residues are highlighted using green spheres. The unit number for each of the residues is indicated next to the residue. B) Electrostatic energy gap fluctuation for the oxidation half reaction computed for equivalent tyrosine residues from the eight repeat subunits of CTPR. The distributions have been normalized.

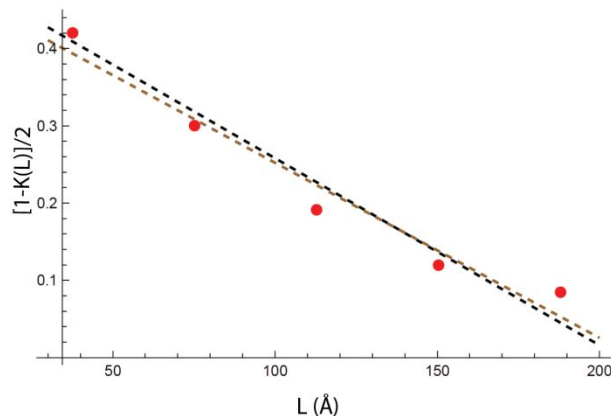


Figure S2: Linear fit to the experimentally-determined bias distribution. $K(L)$ is the fraction of the applied bias that appears across the molecule. The potential drop at the contacts is $\eta(L) = V_b \frac{1-K(L)}{2} \approx V_b(0.5 - 0.02042L/\text{\AA})$.

Stokes-shift and Distance Dynamics

The dynamical crossover parameter g accounts for the solvent dynamical control of the rate pre-exponential factor. Equation S1 shows that g includes two relaxation times: the integral relaxation times τ_X for the Stokes-shift dynamics and the relaxation time τ_R for the dynamics of the donor-acceptor distance⁷

$$g = \frac{2\pi V_{DA}^2 \tau_X}{\sigma_X \hbar} \frac{e^{\frac{3}{2}\gamma^2 \langle (\delta R)^2 \rangle}}{\sqrt{2\beta F_{act} + 4(\tau_X/\tau_R)\gamma^2 \langle (\delta R)^2 \rangle}} \quad (\text{S1})$$

In addition, $\sigma_X^2 = 2k_B T \lambda$, γ is the parameter of the exponential fall-off of the squared donor-acceptor electronic coupling and $\langle (\delta R)^2 \rangle$ is the distance variance.

The Hopfield equation⁸ used to calculate V_{DA} is based on the edge-to-edge distance (R_{edge} , in nm) between the donor and acceptor

$$V_{DA} = \frac{2.7eV}{\sqrt{N_A N_D}} e^{-7.2R_{edge}} \quad (\text{S2})$$

Here $N_{D,A} = 7$ for tyrosine and $N_{D,A} = 9$ for tryptophan. In addition, the activation energy ΔG^\ddagger in Eq. 1 is calculated as

$$\Delta G^\ddagger = \frac{(\lambda^r \pm \Delta G)^2}{4\lambda^r} \quad (\text{S3})$$

with “+” and “-” referring to the forward and backward transitions. In Eq. S3, λ^r is the reaction (superscript “r”) reorganization energy calculated from the equation⁹

$$\lambda^r = (\lambda^{St})^2 / \lambda \quad (S4)$$

where the variance reorganization energy $\lambda = \sigma_X^2 / 2k_B T$ is calculated from the variance of the energy gap reaction coordinate X . We take the mean of the forward and backward λ to calculate the reaction reorganization energy λ^r in Eq. S4. The Stokes-shift reorganization energy λ^{St} is given by the difference of average values of the energy gap in the initial and final electron-transfer states

$$\lambda^{St} = \frac{|\langle X \rangle_1 - \langle X \rangle_2|}{2} \quad (S5)$$

Calculations of the Stokes-shift and donor-acceptor distance dynamics were based on MD simulations using NAMD² with a 4 fs integration time step and with hydrogen mass repartition.¹⁰ Simulations in the NPT ensemble were performed using a Langevin dynamics thermostat and the Nose-Hoover Langevin^{4,5} piston pressure control set at 310 K and 1 atm. The Stokes-shift dynamics were calculated using two MD trajectories, one being 1 ns in duration and sampled every 12 fs and another being 250 ns in duration and sampled every 10 ps. Both simulation systems probed the same electron transfer reaction between oxidized residue Y43 and neutral Y77. The energy gap was calculated as a function of time for the short and long trajectories. The two trajectories were combined while disposing the first 1 ns of the longer trajectory. The Stokes-shift correlation function $C_X(t) = \langle \delta X(t) \delta X(0) \rangle$ was normalized and fitted to a sum of a Gaussian ballistic decay and two exponential functions

$$S_X(t) = \frac{C_X(t)}{C_X(0)} = (1 - a - b)e^{-t^2/\lambda_1} + ae^{-t/\lambda_2} + be^{-t/\lambda_3} \quad (S6)$$

The MD data and the fit are shown in Fig S3. The fit was obtained with the parameters: $a = 0.085$, $b = 0.662$, $\lambda_1 = 0.0777 \text{ ns}^2$, $\lambda_2 = 3.8 \times 10^{-3} \text{ ns}$, and $\lambda_3 = 6 \times 10^{-5} \text{ ns}$. These fitting parameters give the integral relaxation time of 20 ps.

The relaxation time for the dynamics of the donor-acceptor distance was calculated from a 65 ns trajectory. The center-of mass distance $R(t)$ between Y55—Y76 residue pair was sampled with the time step of 2.5 ps producing the correlation function

$$S_R(t) = \frac{C_R(t)}{C_R(0)} = e^{-2.953t^{0.27}} \quad (S7)$$

where $C_R(t) = \langle \delta R(t) \delta R(0) \rangle$. The result is shown in Fig S4. The fit to Eq. S7 yields the integral relaxation time $\tau_R = 281 \text{ ps}$.

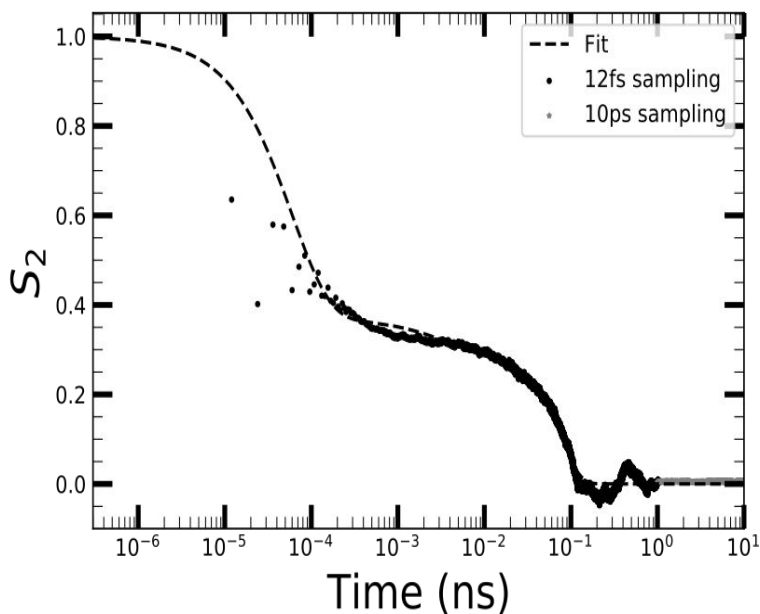


Figure S3: Stokes-shift time correlation function. The dots and stars are the data from MD simulation, while the dashed line indicates the fit to Eq. 6. The grey stars indicate correlation data from 10ps sampling step and the black dots indicate correlation data during the 12fs step.

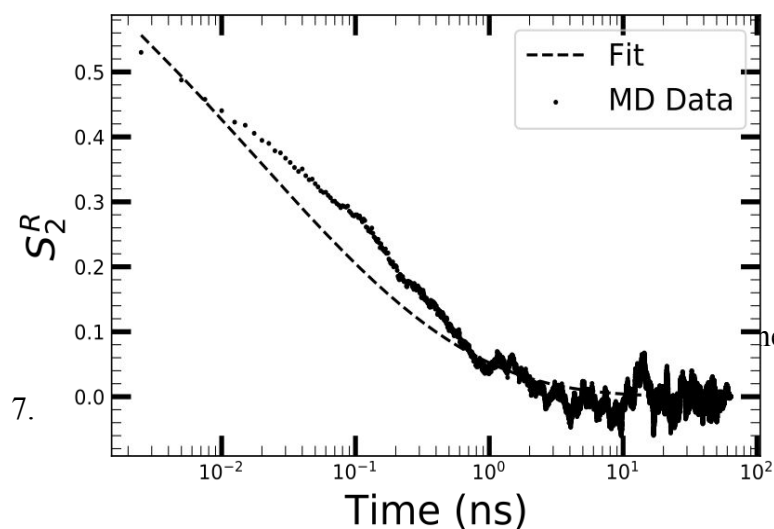


Figure S4: Distance time correlation function. The dots are the data from MD simulation, while the dashed line indicates the fit to Eq.

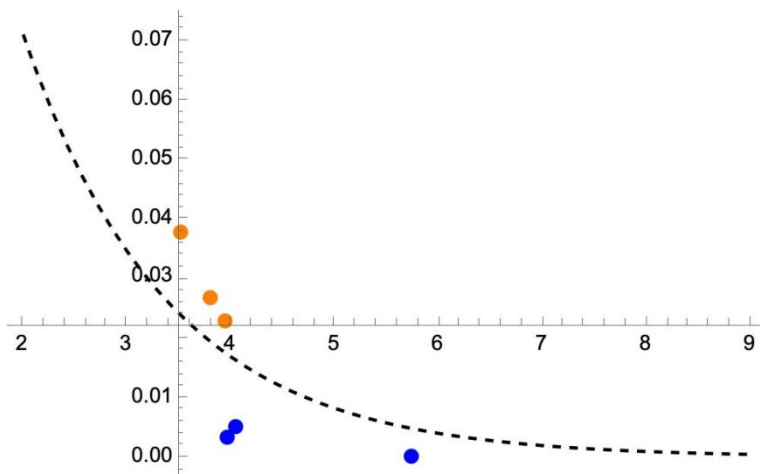


Figure S5: Hopfield equation(dashed) and direct ab initio calculations of V_{DA} (eV) from Cailliez et al.¹ (orange) and Ludemann et al.² (blue). The distance is edge-to-edge between two Trp residues in Angstroms.

Polarizability

We conduct the MD simulations in non-polarizable force fields, which do not account for screening of electrostatic interaction by electronic induced dipole moments. The standard dielectric theories account for the medium polarization in terms of the Pekar factor $c_0 = \frac{1}{\epsilon_\infty} - \frac{1}{\epsilon_s}$ which results in the reduction of the reorganization energy by a factor ≈ 2 when the dielectric constant due to induced dipole ϵ_∞ is accounted for (ϵ_s is the static dielectric constant).

Microscopic simulations and analytical theories^{11,12,13} indicate that the reduction is smaller than suggested by continuum theories, but the problem has not been studied in depth for protein electron transfer.¹⁴ With ϵ_∞ of water, the reduction compared to nonpolarizable solvents is 0.8 and this factor was used here to rescale the reorganization energies from MD simulations. The corrected λ and λ^{St} are the MD values (Table S1) multiplied by a factor of 0.8. As the result of this correction, the reaction reorganization energy in Eq 5 is also multiplied by 0.8.

Rate Calculations

Applying both relaxation times to Eq S1, we find that, due to a large relaxation time of distance fluctuations $\tau_R = 281$ ps, the term including τ_X/τ_R in the denominator of Eq. 1 can be dropped. A simpler result for the crossover parameter g follows

$$g = \frac{\pi V_{DA}^2 \tau_X}{\hbar \sqrt{\lambda F_{act}}} e^{\frac{3}{2} \gamma^2 \langle (\delta R)^2 \rangle} \quad (\text{S8})$$

We also find that the parameter g is large, $g \approx 55$ at $R \approx 0.6$ nm, when $\gamma = 14.4 \text{ nm}^{-1}$ and $\langle (\delta R)^2 \rangle = 0.041^2 \text{ nm}^{-1}$ are adopted. The parameter γ is taken from the Hopfield equation (Eq. S2) used to calculate the electronic coupling and the variance of the donor-acceptor distance is from MD

simulations of the Y55-Y76 pair adopted for all other donor-acceptor pairs. This value of g implies that, at relatively short distances, electron hops between the residues are in the dynamics controlled regime when the rate constant is not affected by the electronic coupling. This happens because the total reaction rate includes the parameter g in the denominator of the following relation

$$k = k_{NA}/(1 + g) \quad (\text{S9})$$

Here, k_{NA} is the non-adiabatic rate constant given by the equation

$$k_{NA} = \frac{V_{DA}^2}{\hbar} \sqrt{\frac{\pi}{k_B T \lambda^r}} \exp\left[\frac{1}{2} \gamma^2 \langle (\delta R)^2 \rangle - \frac{\Delta G^\ddagger}{k_B T}\right] \quad (\text{S10})$$

The dynamics-controlled electron-transfer rate constant becomes

$$k = \frac{1}{\tau_X} \sqrt{\frac{\Delta G^\ddagger}{k_B T \pi}} e^{-\gamma^2 \langle (\delta R)^2 \rangle - \frac{\Delta G^\ddagger}{k_B T}} \quad (\text{S11})$$

The rate calculations between pairs of residues (Table S1) produce the parameter g spanning a broad range of values such that both the dynamics-controlled and nonadiabtic limits apply to specific intra-protein electron hops. The appearance of the crossover parameter g in the form given by Eqs. S1 and S8 leads to slight deviations from the detailed balance condition requiring the ratio of the forward and backward rate constant to be equal to the Boltzmann factor $\exp[-\beta \Delta G]$. Given that the Derrida model used here for the calculation of the carriers diffusion constant requires detailed balance, we used a somewhat simplified form of the parameter g replacing ΔG^\ddagger in Eqs. 1 and 9 with $\lambda^r/4$. The correction is mostly insignificant for the rate values, but strictly preserves the detailed balance.

Diffusion constant from the Derrida model

Following Derrida¹⁷

$$D = \frac{N \Delta x^2}{\sum_{n=1}^N r_n} \sum_{n=1}^N k_{n+1,n} r_n u_n \quad (\text{S12})$$

where the step size Δx is calculated as the average distance between the residues and

$$r_n = \frac{1}{k_{n+1,n}} \left[1 + \sum_{i=1}^{N-1} \prod_{j=1}^i \frac{k_{n+j-1,n+j}}{k_{n+j+1,n+j}} \right] \quad (\text{S13})$$

$$u_n = \frac{1}{k_{n+1,n}} \left[1 + \sum_{i=1}^{N-1} \prod_{j=1}^i \frac{k_{n-j,n+1-j}}{k_{n+1-j,n-j}} \right]$$

Applied to the path listed in Table S3, these equations yield $D = 3.06 \text{ nm}^2/\text{ns}$. Similar numbers are found for other single paths. Applied to the 433 such paths connecting Y36 to Y89, we obtain a sum of the 433 D values of $578 \text{ nm}^2/\text{ns}$.

Charge Injection Calculation

The rate constants for the two contact sites, 1, 2 are

$$k_R^{1,2} = \frac{\Delta}{\hbar} \text{erfc} \left(\frac{\lambda^r \mp e\eta}{\sqrt{4\lambda^r k_B T}} \right) \quad (\text{S14})$$

$$k_O^{1,2} = \frac{\Delta}{\hbar} \text{erfc} \left(\frac{\lambda^r \pm e\eta}{\sqrt{4\lambda^r k_B T}} \right)$$

where R and O refer to reduction or oxidation and we assume the same electronic coupling to the contacts, Δ , and the potential drop at the contacts, η , is given in the caption to Figure S2. “-“ and “+” refer to 1 and 2, respectively.

The kinetic equation for the fraction of holes n at the single injection site is

$$\partial_t n(x) = k_R c_s n(x) - k_O c_s (1 - n(x)) \quad (\text{S15})$$

Where $k_R = k_R^1 + k_R^2$ and $k_O = k_O^1 + k_O^2$ and $c_s = I/S$ is the surface concentration determined by the area of the contact, S . At the stationary condition determined by $\partial_t n(x) = 0$, one gets $n = \frac{1}{2}$ and the following expression for the total current I through the contact

$$I = \frac{e\Delta}{\hbar} \left[\text{erfc} \left(\frac{\lambda^r - e\eta}{\sqrt{4\lambda^r k_B T}} \right) - \text{erfc} \left(\frac{\lambda^r + e\eta}{\sqrt{4\lambda^r k_B T}} \right) \right] \quad (\text{S16})$$

Kinetic Monte Carlo Model and Brownian diffusion : We perform single charge kinetic Monte Carlo based on a previous routine implemented in python²¹ to simulate charge hopping in

the graph based representation of the protein. Each node in the graph is connected by two edges, one for forward and one for backward rates. Every iteration of the Monte Carlo involves determining the lifetime of the charge on the node i which it currently resides on and the node which the charge hops to next. The charge can only hop to the site which are connected to its current node by an edge. First, the lifetime of the charge τ is determined from an exponential random variable T as $\tau = T/\Gamma_i$, where Γ_i is the sum of the weights of the edges which originate at node i .

$$\Gamma_i = \sum_j \Gamma_{ij} \quad (\text{S17})$$

Γ_{ij} is the weight of the edge connecting nodes i to j which is essentially the rate of charge transfer between the residues represented by i and j . Next, to determine which residue, the charge hops to, we calculate the probability of hopping to that residue/node j .

$$p_{ij} = \frac{\Gamma_{ij}}{\Gamma_i} \quad (\text{S18})$$

A random number u is drawn from a uniform distribution and the next site k is determined from the inequality.

$$\sum_{j < k} p_{ij} \leq u < \sum_{j \leq k} p_{ij} \quad (\text{S19})$$

The Monte Carlo (MC) simulation ends when the charge arrives at the residue in the protein which is in contact with the electrodes. We store the residence time τ for every hop and the distance Δx_i between the center of mass of the residue sidechains travelled during every hop. We then calculate the average Brownian diffusion for that path.

$$D = \langle \Delta x_i^2 / 2\tau_i \rangle \quad (\text{S20})$$

The diffusion constant is calculated for 100000 MC with the starting residue as W35. Another 100000 MC runs are performed for Y36 as the starting residue, summarized Figure 6 of the main text. The resultant diffusion constant values are divided into 300 bins to obtain a distribution, which is fit to a gamma function probability distribution function given by the expression

$$PDF(x) = \frac{e^{-\frac{x}{\beta}} x^{-1+\alpha} \beta^{-\alpha}}{\Gamma[\alpha]} \quad (S21)$$

Here α and β are parameters which determine the skewness and peak location of the distribution respectively. We assume β to be the effective diffusion constant for the transport. This gives us 22.13 nm²/ns for W35 and 22.8 nm²/ns for Y36.

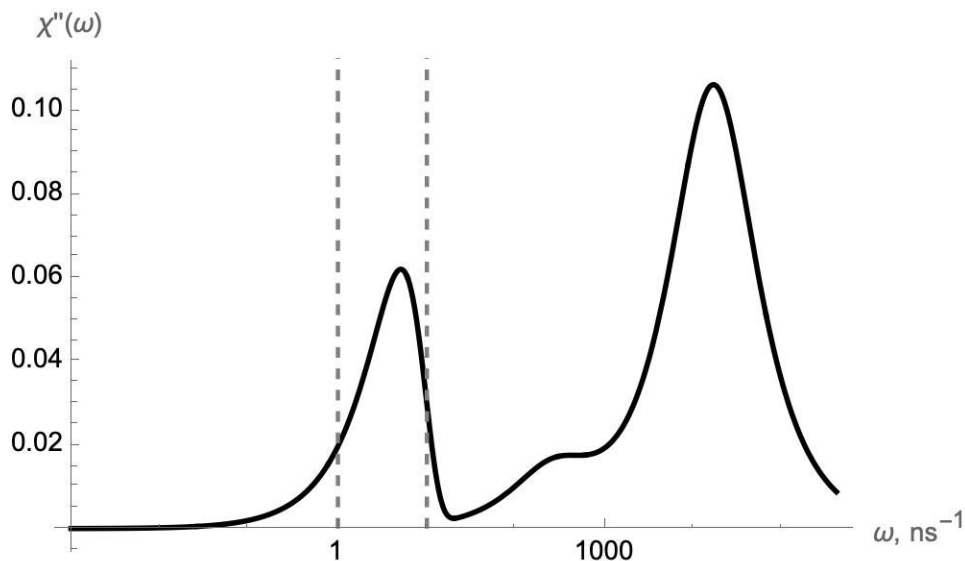


Figure S6: Loss spectrum of the Stokes-shift dynamics calculated from the Stokes-shift correlation function (Eq. (S6)) reported by MD simulations. The two dashed vertical lines refer to the rate constants of 1 and 10 ns⁻¹. Most electron hops reported here fall in this interval.

The Stokes-shift correlation function $S_X(t)$ in Eq. (S6) is used to calculate the Laplace-Fourier transform $S_X(\omega)$ and the loss function shown in Figure S6

$$\chi''(\omega) = 2\lambda' \text{Re}[\omega S_X(\omega)] \quad (S22)$$

| Acceptor | Donor | $\lambda^{St}(eV)$ | $\lambda_{var}(eV)$ | $\Delta G(eV)$ | Edge Distance (\AA) | λ^r |
|----------|-------|--------------------|---------------------|----------------|--------------------------------|-------------|
| 35 | 36 | 0.55 | 1.422 | 0.18 | 4.51 | 0.213 |
| 35 | 42 | 0.561 | 1.482 | 0.18 | 9.097 | 0.212 |
| 35 | 43 | 0.632 | 1.834 | 0.18 | 11.542 | 0.217 |
| 35 | 54 | 0.543 | 0.881 | 0.18 | 3.437 | 0.335 |
| 35 | 55 | 0.756 | 1.3 | 0.18 | 5.45 | 0.44 |
| 36 | 42 | 0.407 | 1.634 | 0.0 | 9.529 | 0.101 |
| 36 | 43 | 0.514 | 1.3 | 0.0 | 8.49 | 0.203 |
| 36 | 54 | 0.484 | 1.561 | 0.0 | 6.674 | 0.15 |
| 36 | 55 | 0.477 | 0.584 | 0.0 | 2.421 | 0.39 |
| 42 | 43 | 0.456 | 1.249 | 0.0 | 4.85 | 0.166 |
| 42 | 48 | 0.383 | 1.756 | 0.0 | 6.683 | 0.083 |
| 42 | 54 | 0.301 | 0.582 | 0.0 | 7.124 | 0.156 |
| 42 | 55 | 0.492 | 1.253 | 0.0 | 7.069 | 0.193 |
| 43 | 48 | 0.348 | 1.312 | 0.0 | 3.419 | 0.092 |
| 43 | 54 | 0.55 | 1.351 | 0.0 | 8.177 | 0.224 |
| 43 | 55 | 0.411 | 0.617 | 0.0 | 4.136 | 0.274 |
| 48 | 54 | 0.51 | 1.871 | 0.0 | 10.181 | 0.139 |
| 48 | 55 | 0.518 | 1.115 | 0.0 | 5.98 | 0.24 |
| 54 | 55 | 0.542 | 1.232 | 0.0 | 4.737 | 0.239 |
| 36 | 69 | 0.631 | 1.42 | -0.18 | 8.594 | 0.28 |
| 36 | 70 | 0.382 | 1.211 | 0.0 | 7.384 | 0.12 |
| 36 | 88 | 0.542 | 1.589 | 0.0 | 9.799 | 0.185 |
| 43 | 70 | 0.465 | 1.512 | 0.0 | 7.35 | 0.143 |
| 43 | 76 | 0.528 | 1.235 | 0.0 | 7.441 | 0.225 |
| 43 | 77 | 0.524 | 1.15 | 0.0 | 6.308 | 0.239 |
| 43 | 88 | 0.529 | 1.364 | 0.0 | 10.328 | 0.205 |
| 43 | 89 | 0.645 | 1.521 | 0.0 | 6.903 | 0.274 |
| 48 | 70 | 0.328 | 1.529 | 0.0 | 12.525 | 0.07 |
| 48 | 76 | 0.465 | 1.677 | 0.0 | 7.543 | 0.129 |
| 48 | 77 | 0.462 | 1.535 | 0.0 | 8.233 | 0.139 |
| 55 | 69 | 0.809 | 1.3 | -0.18 | 6.901 | 0.503 |
| 55 | 70 | 0.544 | 0.983 | 0.0 | 9.022 | 0.301 |
| 55 | 76 | 0.654 | 1.087 | 0.0 | 6.001 | 0.393 |
| 55 | 77 | 0.45 | 0.964 | 0.0 | 8.64 | 0.21 |
| 55 | 88 | 0.697 | 1.126 | 0.0 | 7.775 | 0.432 |
| 55 | 89 | 0.768 | 0.949 | 0.0 | 8.734 | 0.621 |

1. **Table S1:** Acceptor (first column) and donor (second column) residue numbers and the reorganization energies calculated from directly from the MD simulations without accounting for the polarization. Also listed (sixth column) the edge-to-edge distance between the residue pairs used in the Hopfield equation. The last column lists the reaction reorganization energies. The edge-to-edge distance is evaluated by finding the pair of atoms with the least cartesian distance in the residues involved in the hop. This distance is assigned as the edge-to-edge distance. The distance is calculated for every frame of the

trajectory. We then calculate the average of the quantity over 30ns between the residue pair involved in the hop.

| | Donor | Acceptor | Forward Rate (/ns) | Backward Rate (/ns) | g | R (nm) |
|-----------|--------------|-----------------|---------------------------|----------------------------|----------|---------------|
| 1 | 35 | 36 | 0.024 | 25.621 | 325.759 | 1.08 |
| 2 | 35 | 42 | 0.007 | 7.848 | 0.441 | 1.09 |
| 3 | 35 | 43 | 0.0 | 0.327 | 0.012 | 1.61 |
| 4 | 35 | 54 | 0.023 | 24.311 | 975.706 | 0.59 |
| 5 | 35 | 55 | 0.015 | 15.964 | 41.042 | 1.03 |
| 6 | 36 | 42 | 3.183 | 3.183 | 0.628 | 1.27 |
| 7 | 36 | 43 | 3.072 | 3.072 | 1.42 | 1.02 |
| 8 | 36 | 54 | 6.589 | 6.589 | 26.219 | 1.15 |
| 9 | 36 | 55 | 1.702 | 1.702 | 4661.247 | 0.55 |
| 10 | 42 | 43 | 6.31 | 6.31 | 327.05 | 1.06 |
| 11 | 42 | 48 | 8.476 | 8.476 | 45.609 | 1.07 |
| 12 | 42 | 54 | 6.165 | 6.165 | 13.142 | 0.65 |
| 13 | 42 | 55 | 5.081 | 5.081 | 11.552 | 1.03 |
| 14 | 43 | 48 | 8.481 | 8.481 | 4563.516 | 0.51 |
| 15 | 43 | 54 | 3.125 | 3.125 | 2.025 | 1.25 |
| 16 | 43 | 55 | 3.502 | 3.502 | 559.671 | 0.69 |
| 17 | 48 | 54 | 1.095 | 1.095 | 0.18 | 1.28 |
| 18 | 48 | 55 | 4.176 | 4.176 | 44.744 | 1.00 |
| 19 | 54 | 55 | 4.293 | 4.293 | 269.791 | 0.86 |
| 20 | 36 | 69 | 11.08 | 0.01 | 0.692 | 1.06 |
| 21 | 36 | 70 | 7.127 | 7.127 | 11.684 | 1.16 |
| 22 | 36 | 88 | 1.104 | 1.104 | 0.237 | 1.37 |
| 23 | 43 | 70 | 6.422 | 6.422 | 10.354 | 1.06 |
| 24 | 43 | 76 | 3.963 | 3.963 | 5.817 | 1.14 |
| 25 | 43 | 77 | 4.153 | 4.153 | 28.054 | 1.05 |

| | | | | | | |
|-----------|----|----|-------|-------|--------|------|
| 26 | 43 | 88 | 0.469 | 0.469 | 0.099 | 1.42 |
| 27 | 43 | 89 | 3.208 | 3.208 | 10.422 | 1.25 |
| 28 | 48 | 70 | 0.104 | 0.104 | 0.011 | 1.42 |
| 29 | 48 | 76 | 6.703 | 6.703 | 8.679 | 1.10 |
| 30 | 48 | 77 | 5.376 | 5.376 | 2.989 | 1.06 |
| 31 | 55 | 69 | 9.752 | 0.009 | 4.441 | 1.01 |
| 32 | 55 | 70 | 0.918 | 0.918 | 0.447 | 1.09 |
| 33 | 55 | 76 | 1.606 | 1.606 | 26.667 | 0.94 |
| 34 | 55 | 77 | 2.653 | 2.653 | 1.108 | 1.39 |
| 35 | 55 | 88 | 0.845 | 0.845 | 1.888 | 1.04 |
| 36 | 55 | 89 | 0.089 | 0.089 | 0.33 | 1.25 |

Table S2: Acceptor (second column) and donor (third column) residue numbers and forward (4th column) and backward rate (5th column). The 6th column lists the crossover parameter g and the last column lists the average COM-COM distance between the residues (averaged over 3000 MD frames). The rates have been calculated with the adjusted reorganization energy to account for the non-polarizable MD forcefield which was used.

| n | Residue Pairs | Forward Rate (ns ⁻¹) | Backward Rate (ns ⁻¹) | g |
|---|---------------|----------------------------------|-----------------------------------|---------|
| 1 | 35-36 | 0.024 | 25.621 | 325.759 |
| 2 | 36-43 | 3.072 | 3.072 | 1.42 |
| 3 | 43-89 | 3.208 | 3.208 | 10.422 |
| 4 | 89-35 | 9.752 | 0.009 | 4.441 |

Table S3: Forward and backward rates and the crossover parameter g for transitions in a path from the start of first unit of CTPR8 protein to the last active residue in the second CTPR8 protein. The path was calculated using Dijkstra's shortest path algorithm¹³. Derrida's model¹⁶ is applied to the path to calculate the diffusion constant of 3.06 nm²/ns.

| Atom | Charge (e) |
|------|----------------------|
| CB | -0.18000000715255737 |
| HB1 | 0.09000000357627869 |
| HB2 | 0.09000000357627869 |
| CG | 0.42800000309944153 |
| CD1 | -0.23000000417232513 |
| HD1 | 0.22300000488758087 |
| CE1 | -0.23000000417232513 |
| HE1 | 0.22300000488758087 |
| CZ | 0.6209999918937683 |
| OH | -0.4300000071525574 |
| HH | 0.4090000092983246 |
| CD2 | -0.23000000417232513 |
| HD2 | 0.22300000488758087 |
| CE2 | -0.23000000417232513 |
| HE2 | 0.11500000208616257 |

Table S4 : Partial charges for Y-H⁺ in units of the elementary charge¹⁹. Atom names are consistent with the CHARMM36 convention. The total sum of the partial charges is +1. The partial charges are applied to the residue and the protein is simulated using NAMD. The trajectory is used to calculate the electrostatic potential map of either the initial or final state during the charge transfer process. The initial state has the electron acceptor residue positively charged while the final state has the donor residue positively charged.

| Atom | Charge (e) |
|------|-----------------------|
| CB | 0.07000000029802322 |
| HB1 | 0.009999999776482582 |
| HB2 | 0.009999999776482582 |
| CG | 0.11999999731779099 |
| CD1 | 0.12999999523162842 |
| HD1 | 0.004999999888241291 |
| NE1 | -0.14000000059604645 |
| HE1 | 0.4699999988079071 |
| CE2 | -0.009999999776482582 |
| CD2 | -0.07000000029802322 |
| CE3 | 0.029999999329447746 |
| HE3 | 0.004999999888241291 |
| CZ3 | 0.15000000596046448 |
| HZ3 | 0.029999999329447746 |
| CZ2 | 0.12999999523162842 |
| HZ2 | 0.004999999888241291 |
| CH2 | 0.05000000074505806 |
| HH2 | 0.004999999888241291 |

Table S5 Partial charges for W-H⁺ in units of the elementary charge²⁰. Atom names are consistent with the CHARMM36 convention. The total sum of the partial charges is +1. The partial charges are applied to the residue and the protein is simulated using NAMD. The trajectory is used to calculate the electrostatic potential map of either the initial or final state during the charge transfer process. The initial state has the electron acceptor residue positively charged while the final state has the donor residue positively charged.

References:

- (1) Jorgensen, W. L.; Chandrasekhar, J.; Madura, J. D.; Impey, R. W.; Klein, M. L. Comparison of Simple Potential Functions for Simulating Liquid Water. 1983, 79, 926–935.
- (2) Phillips, J. C.; Braun, R.; Wang, W.; Gumbart, J.; Tajkhorshid, E.; Villa, E.; Chipot, C.; Skeel, R. D.; Kale, L.; Schulten, K. Scalable molecular dynamics with NAMD. 2005, 26, 1781–1802.
- (3) Aksimentiev, A.; Schulten, K. Imaging α -Hemolysin with Molecular Dynamics: Ionic Conductance, Osmotic Permeability and the Electrostatic Potential Map. 2005, 88, 3745–3761.
- (4) Nosé, S.; Klein, M. L. Constant Pressure Molecular Dynamics for Molecular Systems. 1983, 50, 1055–76.

- (5) Feller, S. E.; Zhang, Y.; Pastor, R. W.; Brooks, B. R. Constant Pressure Molecular Dynamics Simulation: The Langevin Piston Method. 1995, 103, 4613–4621.
- (6) Huang, J.; Rauscher, S.; Nawrocki, G.; Ran, T.; Feig, M.; de Groot, B. L.; Grubmüller, H.; MacKerell, A. D. CHARMM36m: an improved force field for folded and intrinsically disordered proteins. 2017, 14, 71–73.
- (7) Gupta, S.; Matyushov, D. V., Effects of Solvent and Solute Polarizability on the reorganization Energy of Electron Transfer, *J. Phys. Chem. A.* 2004, 108, 2087.
- (8) Hopfield, J. J., Electron Transfer Between Biological Molecules by Thermally Activated Tunneling. *Proceedings of the National Academy of Sciences* **1974**, 71 (9), 3640-3644.
- (9) Matyushov, D. V. Protein electron transfer: Dynamics and statistics, *J. Chem. Phys.* 139 (2013) 025102.
- (10) Balusek, C.; Hwang, H.; Lau, C. H.; Lundquist, K.; Hazel, A.; Pavlova, A.; Lynch, D. L.; Reggio, P. H.; Wang, Y.; Gumbart, J. C. Accelerating Membrane Simulations with Hydrogen Mass Repartitioning. 2019, 15, 4673–4686.
- (11) Bader, J. S.; Berne, B. J., Solvation spectra and solvation energies in polar, polarizable media: Simulation tests of dielectric continuum, *J. Chem. Phys.* 1996, 104, 1293.
- (12) Dinpajoo, M.; Newton, M. D.; Matyushov, D. V., Free energy functionals for polarization fluctuations: Pekar factor revisited, *J. Chem. Phys.* 2017, 146, 064504.
- (13) Blumberger, J. Recent Advances in the Theory and Molecular Simulation of Biological Electron Transfer Reactions, *Chem. Rev.* 2015, 115, 11191.
- (14) D. V. Matyushov, Conformational dynamics modulating electron transfer. *J. Chem. Phys.* 2022, 157, 095102.
- (15) Ru, X.; Zhang, P.; Beratan, D. N., Assessing Possible Mechanisms of Micrometer-Scale Electron Transfer in Heme-Free *Geobacter sulfurreducens* Pili. *The Journal of Physical Chemistry B* **2019**, 123 (24), 5035-5047.
- (16) Dahl, P. J.; Yi, S. M.; Gu, Y.; Acharya, A.; Shipps, C.; Neu, J.; O'Brien, J. P.; Morzan, U. N.; Chaudhuri, S.; Guberman-Pfeffer, M. J.; Vu, D.; Yalcin, S. E.; Batista, V. S.; Malvankar, N. S., A 300-fold conductivity increase in microbial cytochrome nanowires due to temperature-induced restructuring of hydrogen bonding networks. *Science Advances* 8 (19), eabm7193.
- (17) Derrida, B., Velocity and diffusion constant of a one-dimensional hopping model. *J. Stat.Phys.* **1983**, 31, 433-453.
- (18) Wyatt Bald. 2021. Dijkstra. <https://github.com/wylee/Dijkstra/blob/dev/LICENSE> (2021)
- (19) Popovic, D. M.; Zmiric, A.; Zaric, S. D.; Knapp, E.-W. Energetics of radical transfer in DNA photolyase. 2002, 124, 3775–3782.
- (20) Bernini, C.; Pogni, R.; Ruiz-Duenas, F. J.; Martínez, A. T.; Basosi, R.; Sinicropi, A. EPR parameters of amino acid radicals in *P. eryngii* versatile peroxidase and its W164Y variant computed at the QM/MM level. 2011, 13, 5078–5098.
- (21) GeeksforGeeks. “Print All Paths From a Given Source to a Destination.” *GeeksforGeeks*, 13 July 2022, www.geeksforgeeks.org/find-paths-given-source-destination.
- (22) Shankar1729. “GitHub - Shankar1729/ChargeHoppingMC: Monte Carlo Model for Charge Hopping in Arbitrary Energy Landscapes.” GitHub. Accessed October 22, 2022. <https://github.com/shankar1729/ChargeHoppingMC>.

- 1 Cailliez, F., Müller, P., Firmino, T., Pernot, P. & de la Lande, A. Energetics of Photoinduced Charge Migration within the Tryptophan Tetrad of an Animal (6–4) Photolyase. *Journal of the American Chemical Society* **138**, 1904-1915, doi:10.1021/jacs.5b10938 (2016).
- 2 Lüdemann, G., Woiczikowski, P. B., Kubař, T., Elstner, M. & Steinbrecher, T. B. Charge Transfer in E. coli DNA Photolyase: Understanding Polarization and Stabilization Effects via QM/MM Simulations. *The Journal of Physical Chemistry B* **117**, 10769-10778, doi:10.1021/jp406319b (2013).